Frequency Domain Turbo Equalization for MIMO-CPSC Systems with Large Delay Spreads

Yogendra U. Itankar and A. Chockalingam
Department of ECE, Indian Institute of Science, Bangalore 560012, India

***Abstract*—In this paper, we consider low-complexity turbo equalization for multiple-input multiple-output (MIMO) cyclic prefixed single carrier (CPSC) systems in MIMO inter-symbol interference (ISI) channels characterized by large delay spreads. A low-complexity graph based equalization is carried out in the frequency domain. Because of the reduction in correlation among the noise samples that happens for large frame sizes and delay spreads in frequency domain processing, improved performance compared to time domain processing is shown to be achieved. This improved performance is attractive for equalization in severely delay spread ISI channels like ultrawideband channels and underwater acoustic channels.**

Keywords *– Frequency-domain turbo equalization, MIMO-CPSC systems, MIMO-ISI channels, large delay spreads.*

I. Introduction

Multiple-input multiple-output (MIMO) communications in frequency selective channels are of interest as rates of transmission in wireless channels are on the increase, rendering the channel more and more frequency selective. Indoor ultrawideband channels and underwater acoustic channels exhibit high orders of frequency selectivity [1]-[4]. The selectivity can be quite severe due to large delay spreads, causing severe inter-symbol interference (ISI). For example, in ultrawideband channels in indoor/industrial environment, the number of multipath components (MPC) has been observed to be of the order of tens to hundreds. Number of MPCs ranging from 12 to 120 are common in ultrawideband channels [2],[3]. Orthogonal frequency division multiplexing (OFDM) has been widely employed in MIMO-ISI channels to convert frequency selectivity in the channel impulse response to non-selectivity in order to enable simple reception.

Viewed differently, ISI channels offer opportunities to harness diversity benefits from large number of delayed paths. In an L-length ISI channel, the availability of L copies of the transmitted signal can be exploited to achieve Lth order diversity. To harness this diversity, data can be organized into K-length frames, $K > L$, and equalization can be carried out jointly over the entire frame. Low-complexity equalization that scales well for large K and L then becomes crucial.

Recently, single carrier (SC) block transmission schemes are considered as good alternatives to address the peak-to-average power ratio (PAPR) issue that arises in multicarrier systems [5]-[9]. SC schemes, namely, zero padded SC (ZPSC) and cyclic prefixed SC (CPSC) schemes, have been shown to achieve good performance [7],[9]. In this paper, we consider MIMO-CPSC schemes with large K and L. In MIMO-CPSC systems, the overall MIMO channel includes a fast Fourier transform (FFT) operation so that the transmitted symbols are estimated from the received signal in the frequency domain. Frequency domain (FD) linear equalization including minimum mean square error (MMSE) equalization [6],[8], and decision feedback equalization [10],[11] for single carrier MIMO systems are known. The use of FD equalizers in turbo equalization was investigated in [12],[13]. Though linear equalizers can scale well for large K and L, their performance is far from optimal.

Our contributions in this paper include: i) we present a graph based low-complexity FD equalizer that scales well for large K and L in MIMO-CPSC systems while achieving near-optimal performance, ii) we show that a Gaussian approximation of a scalar sum interference variable in computing the messages in the above equalizer is crucial in achieving both low-complexity as well as near-optimal performance, and that the good performance is due to the reduction in correlation among the noise samples that happens for large K and L in frequency domain processing, and iii) since the graph based equalizer is a soft-input soft-output equalizer, iterative techniques (turbo equalization) between equalization and decoding can yield good coded bit error rate (BER) performance at low complexities in coded systems. We present coded BER performance results of turbo equalization for large K and L with the graph based equalizer for detection and BCJR algorithm for decoding an outer convolutional code. This FD turbo equalizer is shown to achieve much better performance compared to linear equalizers in MIMO-CPSC systems with large K and L, making it attractive for severely delay spread MIMO-ISI channels like ultrawideband and underwater acoustic channels.

II. System Model

Consider a coded communication system where the information bit sequence $\{a_n\}$ is encoded into a coded bit stream $\{b_n\}$ using a code of rate r. Let B denote the number of information bits per frame so that B/r denote the number of coded bits per frame. An interleaver scrambles the coded bit sequence $\{b_n\}$ into a interleaved bit sequence $\{c_n\}$, which is BPSK modulated to get the modulated symbol sequence $\{x_n\}$, $x_n = (-1)^{c_n}$. The modulated symbol stream $\{x_n\}$ is divided into n_t-length vectors, and each of these vectors is transmitted in one independent channel use on n_t transmit

This work was supported in part by a gift from The Cisco University Research Program, a corporate advised fund of Silicon Valley Community Foundation.

978-1-4673-0990-5/12/$31.00 ©2012 IEEE

antennas using spatial multiplexing. For a frame consisting of B/r coded bits, the number of data channel uses per frame K is, $K = B/rn_t$.

Consider a MIMO channel with n_t transmit and n_r receive antennas, where the channel between each pair of transmit and receive antennas is assumed to be frequency selective with L multipath components (MPC). We consider CPSC signaling, where the K data channel uses are preceded by a cyclic prefix (CP) of length $L-1$ channel uses, $K \geq L$, so that each frame has a total of $K' = K + L - 1$ channel uses. Let $\mathbf{x}_q \in \{\pm 1\}^{n_t}$ denote the data symbol vector transmitted in the qth channel use, $q = 0, 1, \cdots, K-1$. The CP vectors avoid the inter-frame interference. But there will be ISI within a frame. The received signal vector at time q can be written as

$$\mathbf{y}_q \;=\; \sum_{l=0}^{L-1} \mathbf{H}_l\, \mathbf{x}_{q-l} + \mathbf{w}_q, \qquad q = 0, \cdots, K-1, \quad (1)$$

where $\mathbf{y}_q \in \mathbb{C}^{n_r}$, $\mathbf{H}_l \in \mathbb{C}^{n_r \times n_t}$ is the channel gain matrix for the lth MPC such that $H_{j,i}^{(l)}$ denotes the entry on the jth row and ith column of the $\mathbf{H}_l$ matrix, i.e., $H_{j,i}^{(l)}$ is the channel from ith transmit antenna to the jth receive antenna on the lth MPC. The entries of $\mathbf{H}_l$ are assumed to be i.i.d $\mathbb{C}\mathcal{N}(0,1)$. It is further assumed that $\mathbf{H}_l$, $l = 0, \cdots, L-1$ remain constant for one frame duration, and vary i.i.d from one frame to the other. $\mathbf{w}_q \in \mathbb{C}^{n_r}$ is the additive white Gaussian noise vector at time q, whose entries are independent, each with variance $\sigma^2 = n_t L E_s/\gamma$, where E_s is the symbol energy and γ is the average received SNR per received antenna. The CP will render the linearly convolving channel into a circularly convolving one. So, the channel will be multiplicative in frequency domain. Because of the CP, the received signal in frequency domain, for the ith frequency index ($0 \leq i \leq K-1$), can be written as

$$\mathbf{r}_i \;=\; \mathbf{G}_i\; \mathbf{u}_i + \mathbf{v}_i, \qquad (2)$$

where $\mathbf{r}_i = \frac{1}{\sqrt{K}} \sum_{q=0}^{K-1} e^{\frac{-2\pi \mathbf{j} qi}{K}} \mathbf{y}_q$, $\mathbf{u}_i = \frac{1}{\sqrt{K}} \sum_{q=0}^{K-1} e^{\frac{-2\pi \mathbf{j} qi}{K}} \mathbf{x}_q$, $\mathbf{v}_i = \frac{1}{\sqrt{K}} \sum_{q=0}^{K-1} e^{\frac{-2\pi \mathbf{j} qi}{K}} \mathbf{w}_q$, $\mathbf{G}_i = \sum_{l=0}^{L-1} e^{\frac{-2\pi \mathbf{j} li}{K}} \mathbf{H}_l$, and $\mathbf{j} = \sqrt{-1}$. Stacking the K vectors $\mathbf{r}_i$, $i = 0, \cdots, K-1$, we get an equivalent linear vector channel model of the form

$$\mathbf{r} \;=\; \underbrace{\mathbf{G}\mathbf{F}}_{\triangleq\, \mathbf{H}} \mathbf{x} + \mathbf{v}, \qquad (3)$$

where $\mathbf{r} = [\mathbf{r}_0^T, \mathbf{r}_1^T, \cdots, \mathbf{r}_{K-1}^T]^T$, $\mathbf{x} = [\mathbf{x}_0^T, \mathbf{x}_1^T, \cdots, \mathbf{x}_{K-1}^T]^T$, $\mathbf{v} = [\mathbf{v}_0^T, \mathbf{v}_1^T, \cdots, \mathbf{v}_{K-1}^T]^T$, $\mathbf{G}$ is block diagonal matrix with $\mathbf{G}_i$'s on its diagonal, i.e., $\mathbf{G} = \mathrm{diag}\{\mathbf{G}_0, \mathbf{G}_1, \cdots, \mathbf{G}_{K-1}\}$, and $\mathbf{F} = \frac{1}{\sqrt{K}} \mathbf{D}_K \otimes \mathbf{I}_{n_t}$, where $\mathbf{D}_K$ is the K-point DFT matrix and $\otimes$ denotes the Kronecker product.

A graph based soft-input soft-output frequency domain equalizer (presented in Sec. III) computes the log-likelihood ratios (LLRs) of the transmitted symbols, which are de-interleaved and then passed to the outer decoder. The decoder computes the LLRs of the code bits and then passes this information to the equalizer after interleaving. At the equalizer, the LLRs from the outer decoder are used as apriori information to compute the new symbol LLRs which are again passed to the decoder. The equalization and decoding steps are repeated for a certain number of iterations. After the final iteration, the decoder computes the estimate of the information bits.

III. Graph Based FD Equalization with Gaussian Approximations

In this section, we consider finding the LLRs for symbol x_k using two types of soft-input soft-output equalizers. One approach is to use a vector Gaussian approximation on the sum interference vector, and the other approach is to use a scalar Gaussian approximation on the scalar sum interference. The vector Gaussian approximation approach, also referred to as the probabilistic data association (PDA) approach [14], approximates the interference-plus-noise (effective noise) vector as a jointly distributed Gaussian random vector. The scalar approach, on the other hand, approximates the effective noise as a scalar Gaussian random variable. The vector approximation approach has high complexity because it involves the inversion of a $Kn_t \times Kn_t$ matrix resulting in $O(K^2 n_t^2)$ per-symbol complexity. Whereas, the scalar approximation approach does not need the above matrix inversion, and needs the computation of only the mean and variance in closed-form that requires only $O(Kn_t)$ per-symbol complexity. Even with one order less complexity, the scalar approach achieves performance which is very close to that of the vector approach (we will see this in Fig. 2). A more detailed presentation of the above two approaches follow.

For simplicity of exposition, here we consider a single transmit and single receive antenna system with L-tap frequency selective channel (a similar treatment follows for MIMO case, and indeed the results in Section IV are for MIMO case). The $\mathbf{G}$ matrix in (3) is a $K \times K$ diagonal matrix made from the K-point DFT of the channel impulse response. The effective channel matrix is $\mathbf{H} = \mathbf{G}\mathbf{F}$, where $\mathbf{F}$ is $K \times K$ DFT matrix.

Vector approximation: Consider the vector approximation approach. Let us consider an arbitrary symbol x_k. Using (3), we have

$$\mathbf{r} \;=\; \mathbf{h}_k x_k + \underbrace{\sum_{j=0, j\neq k}^{K-1} \mathbf{h}_j x_j + \mathbf{v}}_{\mathbf{v}_k}, \qquad (4)$$

where $\mathbf{h}_k$ is the kth column of $\mathbf{H}$ and $\mathbf{v}_k$ is the effective noise vector. Writing $\mathbf{h}_j = \mathbf{G}\mathbf{f}_j$, we have

$$\mathbf{v}_k = \mathbf{G}\Big(\sum_{j=0, j\neq k} \mathbf{f}_j x_j \Big) + \mathbf{v}, \qquad (5)$$

where $\mathbf{f}_j$ is the jth column of FFT matrix $\mathbf{F}$. Assuming independent data symbols, each entry of $\mathbf{v}_k$ is a sum of $K-1$ independent random variables. For large K, the pdf of each entry of $\mathbf{v}_k$ may be approximated by a complex Gaussian distribution so that $\mathbf{v}_k$ approximates a jointly Gaussian

distributed random vector with mean vector $\boldsymbol{\mu}_k$, covariance matrix $\boldsymbol{\Sigma}_k$, and pseudo-covariance matrix $\mathbf{M}_k$:

$$\boldsymbol{\mu}_k = \mathbf{G}\Big(\sum_{j=0,j\neq k}^{K-1} \mathbb{E}(x_j)\mathbf{f}_j\Big), \quad (6)$$

$$\boldsymbol{\Sigma}_k = \mathbf{G}\Big(\sum_{j=0,j\neq k}^{K-1} \text{var}(x_j)\mathbf{f}_j\mathbf{f}_j^H\Big)\mathbf{G}^H + \sigma^2\mathbf{I}_K, \quad (7)$$

$$\mathbf{M}_k = \mathbf{G}\Big(\sum_{j=0,j\neq k}^{K-1} \mathbb{E}(x_j x_j^T)\mathbf{f}_j\mathbf{f}_j^T\Big)\mathbf{G}^T. \quad (8)$$

The algorithm to find the LLR for x_k is iterative in nature. In the first iteration, $P(x_j) = 0.5,\ \forall\ j$. For other iterations, the symbol LLRs computed in the previous iteration are used in (6), (7) and (8). The probability density function the $2K$ dimensional real noise vector $\widetilde{\mathbf{v}}_k = [(\mathcal{R}(\mathbf{v}_k))^T(\mathcal{I}(\mathbf{v}_k))^T]^T$ is given by

$$p(\widetilde{\mathbf{v}}_k) \propto \exp\left\{\frac{-(\widetilde{\mathbf{v}}_k - \widetilde{\boldsymbol{\mu}}_k)^T\widetilde{\boldsymbol{\Gamma}}_k^{-1}(\widetilde{\mathbf{v}}_k - \widetilde{\boldsymbol{\mu}}_k)}{2}\right\}, \quad (9)$$

where the mean vector $\widetilde{\boldsymbol{\mu}}_k = [(\mathcal{R}(\boldsymbol{\mu}_k))^T(\mathcal{I}(\boldsymbol{\mu}_k))^T]^T$ and covariance matrix

$$\widetilde{\boldsymbol{\Gamma}}_k = \frac{1}{2}\begin{bmatrix} \mathcal{R}(\boldsymbol{\Sigma}_k + \mathbf{M}_k) & \mathcal{I}(-\boldsymbol{\Sigma}_k + \mathbf{M}_k) \\ \mathcal{I}(\boldsymbol{\Sigma}_k + \mathbf{M}_k) & \mathcal{R}(\boldsymbol{\Sigma}_k - \mathbf{M}_k) \end{bmatrix}. \quad (10)$$

The log-likelihood for symbol x_k is then given by

$$L_E(x_k) = \ln\frac{P(\widetilde{\mathbf{r}}|x_k = +1)}{P(\widetilde{\mathbf{r}}|x_k = -1)} = \ln\frac{P(\widetilde{\mathbf{v}}_k = \widetilde{\mathbf{r}} - \widetilde{\mathbf{h}}_k)}{P(\widetilde{\mathbf{v}}_k = \widetilde{\mathbf{r}} + \widetilde{\mathbf{h}}_k)}, \quad (11)$$

where $\widetilde{\mathbf{r}} = [(\mathcal{R}(\mathbf{r}))^T(\mathcal{I}(\mathbf{r}))^T]^T$, $\widetilde{\mathbf{h}}_k = [(\mathcal{R}(\mathbf{h}_k))^T(\mathcal{I}(\mathbf{h}_k))^T]^T$ The main computational complexity of (9) comes from the inversion of the $2K \times 2K$ covariance matrix. The LLR for symbol x_k computed in (11) is used to obtain LLR for other symbols $\{x_j, j \neq k\}$ in the next iteration. This is repeated for a certain number of iterations, at the end of which symbol decisions are made.

Scalar approximation: Next, consider the scalar approximation approach. We will treat each entry of the observation vector $\mathbf{r}$ as a factor node and each transmitted symbol x_k as a variable node in a factor graph. Factor node r_i is connected to variable node x_k if $h_{ik} \neq 0$, where h_{ik} is the (i,k)th element of matrix $\mathbf{H}$. Given a factor graph, the LLR for x_k can be found by combining the messages from the connected factor nodes. The received signal r_i (ith element of $\mathbf{r}$) can be written as

$$r_i = h_{ik}x_k + \textstyle\sum_{j=0,j\neq k}^{K-1} h_{ij}x_j + v_i. \quad (12)$$

When computing the message from the ith observation node to the kth variable node, we make the following scalar Gaussian approximation of the interference:

$$r_i = h_{ik}x_k + \underbrace{\sum_{j=0,j\neq k}^{K-1} h_{ij}x_j + v_i}_{\triangleq\ z_{ik}}, \quad (13)$$

where the scalar interference-plus-noise term, z_{ik}, is modeled as $\mathbb{CN}(\mu_{z_{ik}}, \sigma^2_{z_{ik}})$ with

$$\mu_{z_{ik}} = \sum_{j=0,j\neq k}^{K-1} h_{ij}\mathbb{E}(x_j), \quad (14)$$

$$\sigma^2_{z_{ik}} = \sum_{j=0,j\neq k}^{K-1} |h_{ij}|^2\,\text{var}(x_j) + \sigma^2. \quad (15)$$

Note that z_{ik} and $\mu_{z_{ik}}$ are the ith elements of column vectors $\mathbf{v}_k$ and $\boldsymbol{\mu}_k$, respectively, in the vector approximation approach. Also, $\sigma^2_{z_{ik}}$ is the ith element on the diagonal of $\boldsymbol{\Sigma}_k$ in the vector approach. The LLR of symbol x_k at observation node i, denoted by Λ_i^k, can be written as

$$\Lambda_i^k = \ln\frac{P(r_i|\mathbf{H}, x_k = 1)}{P(r_i|\mathbf{H}, x_k = -1)} = \frac{4\Re\left(h_{ik}^*(r_i - \mu_{z_{ik}})\right)}{\sigma^2_{z_{ik}}}. \quad (16)$$

The LLR values computed at the observation nodes are passed to the variable nodes. The message passed from the variable node x_k to factor node r_i, denoted by m_k^i, is computed as

$$\text{m}_k^i = \sum_{l=0,l\neq i}^{K-1} \Lambda_l^k. \quad (17)$$

The probability $p(x_k = +1)$ at factor node i, denoted by p_i^{k+}, is computed as

$$p_i^{k+} = \frac{\exp(\text{m}_k^i)}{1 + \exp(\text{m}_k^i)}. \quad (18)$$

This message passing is carried out for a certain number of iterations. Finally, the LLR for x_k is computed as

$$L_E(x_k) = \sum_{i=0}^{K-1} \Lambda_i^k. \quad (19)$$

In uncoded systems, symbols are detected as $\hat{x}_k = \text{sgn}\left(L_E(x_k)\right)$. In coded systems, $L_E(x_k)$'s are deinterleaved and passed to the decoder.

The approximation of interference as scalar Gaussian in (13) greatly simplifies the computation of messages. Note that there is no need for covariance matrix inversion in this approach. Also, a naive implementation of (16) would require a summation over $K-1$ variable nodes for each message. However, the summation over $K-1$ variables in (14) can be written in the form $\sum_{j=0}^{K-1} h_{ij}\mathbb{E}(x_j) - h_{ik}\mathbb{E}(x_k)$, where the computation of the full summation from $j = 1$ to K (which is independent of the variable index k) requires $K-1$ additions. In addition, one subtraction operation for each k is required. The makes the per-symbol complexity order for computing (14) to be only $O(K)$. A similar argument holds for computation of the variance in (15). Likewise, a similar rewriting of the summation in (17) leads to an overall per-symbol complexity of the algorithm to be only $O(K)$.

Vector versus scalar approximation: In the scalar approximation approach, the effective noise samples, z_{ik}'s, are assumed

to be circularly symmetric r.v's. Now, substituting $\mathbf{M}_k = \mathbf{0}$ in (10) in the vector approximation approach, we get

$$\widehat{\mathbf{\Gamma}}_k \quad = \quad \frac{1}{2}\begin{bmatrix} \mathcal{R}(\mathbf{\Sigma}_k) & \mathcal{I}(-\mathbf{\Sigma}_k) \\ \mathcal{I}(\mathbf{\Sigma}_k) & \mathcal{R}(\mathbf{\Sigma}_k) \end{bmatrix}. \tag{20}$$

If we neglect the off-diagonal elements of $\widehat{\mathbf{\Gamma}}_k$, then we have

$$\overline{\mathbf{\Gamma}}_k = \frac{1}{2}\text{diag}\left\{\sigma^2_{z_{0k}}, \cdots, \sigma^2_{z_{(K-1)k}}, \sigma^2_{z_{0k}}, \cdots, \sigma^2_{z_{(K-1)k}}\right\}. \tag{21}$$

Substituting $\widetilde{\mathbf{\Gamma}}_k = \overline{\mathbf{\Gamma}}_k$ in (9) to compute the LLR for symbol x_k according to (11), we get

$$L_E(x_k) \quad = \quad 4\sum_{i=0}^{K-1} \frac{h^*_{ik}(r_i - \mu_{z_{ik}})}{\sigma^2_{z_{ik}}}, \tag{22}$$

which turns out to be the same as (19) in the scalar approach. Hence, the scalar approximation approach essentially amounts to the vector approximation by forcing the pseudo-covariance matrix and off-diagonal elements in $\widetilde{\mathbf{\Gamma}}_k$ to zero. When K and L are small, the off-diagonal elements in $\widetilde{\mathbf{\Gamma}}_k$ are significant $\big($see Fig. 1(a), where $L = 2$, $K = 10\big)$. However, for large K and L, these elements become small[1] $\big($see Fig. 1(b), where $L = 20, K = 100\big)$, indicating a reduction in the correlation between the effective noise samples for large K and L. Therefore, the loss in performance due to ignoring the off-diagonal terms in the scalar approach for large K and L is expected to be small compared to the vector approximation approach where the off-diagonal terms are not ignored. This is confirmed by the simulated BER plots shown in Fig. 2, where the performance of both vector as well as scalar approximation approaches are found to be very close for $L = 20$, $K = 128$. Also, this performance is seen to be very close to the matched filter bound indicating near-optimal performance. So, we can see that the scalar approach is attractive on two counts compared to the vector approach: 1) ignoring the off-diagonal elements in the covariance matrix reduces the complexity by an order, and 2) the resulting performance loss due to ignoring the off-diagonal elements can be insignificant for large K and L. We further note that a scalar interference approximation has been done in 'time domain (TD)' in [15]. However, the effective noise samples there are correlated $\big($see Fig. 1(c)$\big)$, which results in degraded error performance (as can be seen in Fig. 2).

IV. FD Turbo Equalization Performance

We evaluated the coded BER performance of the turbo equalization scheme which uses the graph based FD equalizer

[1]An analytical explanation for such small off-diagonal terms for large K is as follows. In the first iteration, $\mathbb{E}(x_j) = 0, \text{var}(x_j) = E_s$, Using (7), we have

$$\begin{aligned} \mathbf{\Sigma}_k \quad &= \quad E_s\mathbf{G}\Big(\sum_{j=0, j\neq k}^{K-1} \mathbf{f}_j\mathbf{f}_j^H\Big)\mathbf{G}^H + \sigma^2\mathbf{I}_K \\ &= \quad E_s\mathbf{G}\mathbf{G}^H + \sigma^2\mathbf{I}_K - E_s\mathbf{G}\mathbf{f}_k\mathbf{f}_k^H\mathbf{G}^H. \end{aligned}$$

The (i,j)th element of the matrix $\mathbf{f}_k\mathbf{f}_k^H$ is $\frac{1}{K}\omega^{(i-j)k}$ where, $\omega = e^{\frac{2\pi\sqrt{-1}}{K}}$. The magnitude of off-diagonal terms in the covariance matrix contributed by $\mathbf{G}\mathbf{f}_k\mathbf{f}_k^H\mathbf{G}^H$ become smaller as K increases.

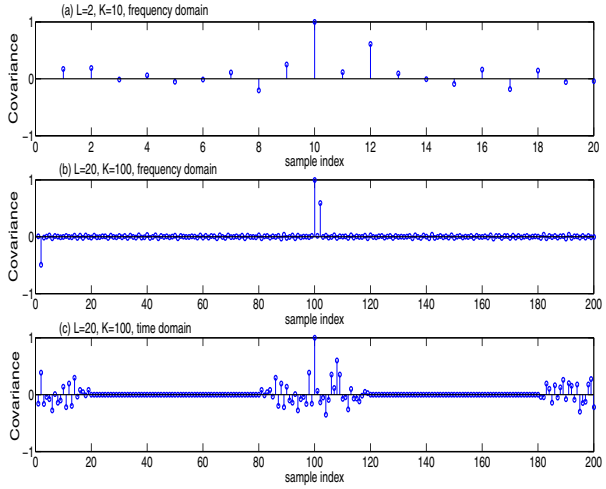

Fig. 1. Normalized covariance $a)$ between 10th element of $\widetilde{\mathbf{v}}_5$ and other elements of $\widetilde{\mathbf{v}}_5$ for $L = 2$, $K = 10$ in frequency domain, $b)$ between 100th element of $\widetilde{\mathbf{v}}_{30}$ and other elements of $\widetilde{\mathbf{v}}_{30}$ for $L = 20$, $K = 100$ in frequency domain, $c)$ between 100th element of $\widetilde{\mathbf{w}}_{30}$ and other elements of $\widetilde{\mathbf{w}}_{30}$ for $L = 20$, $K = 100$ in time domain. Uniform power delay profile, BPSK.

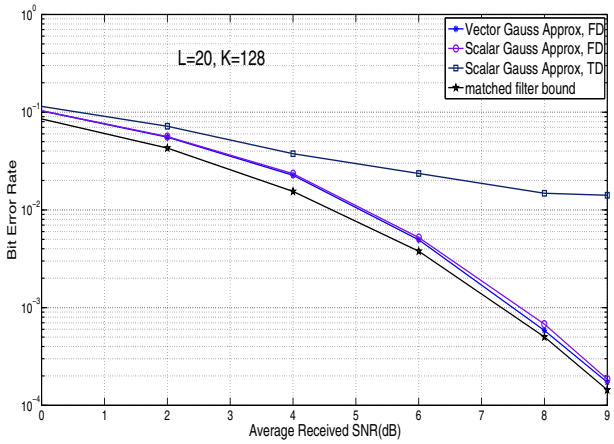

Fig. 2. Uncoded BER performance in single-input single-output CPSC system with $L = 20$, $K = 128$, uniform power delay profile: $i)$ vector approximation approach in FD, 5 iterations, $ii)$ scalar approximation approach in FD, 5 iterations, $iii)$ scalar approximation approach in TD, 5 iterations, and $iv)$ performance of matched filter receiver with no ISI, BPSK.

(scalar approximation) presented in the previous section as the component equalizer and BCJR algorithm as the component decoder. A rate-1/2 convolutional code given by the generator $(1 + D^2,\ 1 + D + D^2)$ is used as the outer code. Random interleaver with $S = 8$ is used. We simulated the coded BER performance in a 4×4 MIMO system with $n_t = n_r = 4$, $L = 20$, $K = 128$ with CPSC signaling. We also compare the performance of the MIMO-CPSC scheme with that of the MIMO-OFDM scheme under the same system parameter settings. Figure 3 shows the coded BER performance plots, where 'Type B' receiver [16] denotes graph based FD equalization followed by decoding without any turbo iteration, and 'Type C' receiver [16] denotes the turbo equalization scheme where multiple iterations between graph based FD equalization and decoding are carried out. In case of MIMO-OFDM, the component equalization is

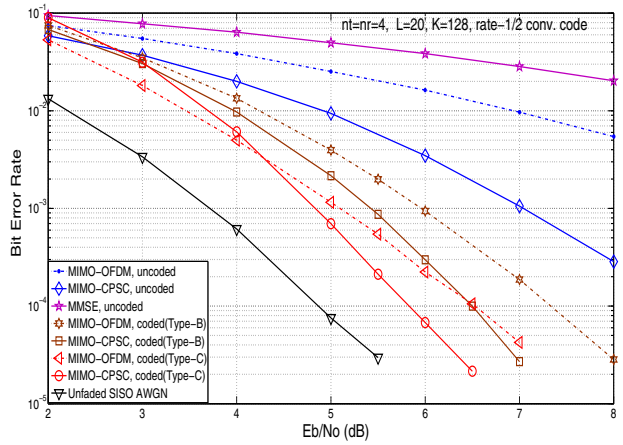

Fig. 3. Coded BER performance of turbo equalization in MIMO-CPSC system with $n_t = n_r = 4$, $L = 20, K = 128$, uniform power delay profile.

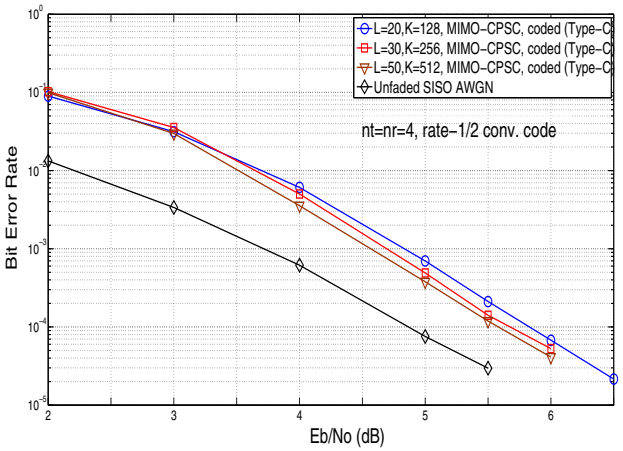

Fig. 4. Coded BER performance of turbo equalization in MIMO-CPSC system with $n_t = n_r = 4$, $(L = 20, K = 128)$, $(L = 30, K = 256)$, and $(L = 50, K = 512)$. Uniform power delay profile.

done using MAP equalizer. The number of local iterations in the graph based FD equalizer in Type B receiver is 5. In Type C receiver, the number of local iterations is 1 and the number of global iterations (between equalizer and decoder) is 6. In addition to coded BER performance, uncoded BER performance of graph based FD equalizer in MIMO-CPSC, performance of MMSE FD equalizer in MIMO-CPSC, and performance of MAP equalizer in MIMO-OFDM are plotted. From Fig. 3, we can observe that the graph based FD equalizer performs significantly better than the linear MMSE FD equalizer (see corresponding uncoded BER plots). In addition, MIMO-CPSC with graph based FD equalizer performs better than MIMO-OFDM with MAP equalizer. It can be seen that turbo equalization (Type C receiver) achieves better coded BER compared to Type B receiver. Also, the Type C receiver performance of MIMO-CPSC is close to (within about 1 dB at 10^{-4}) the performance on unfaded AWGN channel, which is a lower bound on the optimum MIMO receiver performance. Figure 4 shows the turbo equalizer performance in 4×4 V-BLAST MIMO system with $(L = 20, K = 128)$, $(L = 30, K = 256)$ and $(L = 50, K = 512)$, which highlights scalability to large K and L and near-unfaded AWGN performance.

V. Conclusions

We presented a low-complexity turbo equalization scheme for MIMO-CPSC systems in MIMO-ISI channels with large delay spreads. A graph based scheme is used as the component equalizer in the turbo equalization. This graph based scheme exploited the benefit of reduction in correlation among the noise samples that happens in large frame sizes and delay spreads in frequency domain processing, for achieving both low complexity as well as good performance. The graph based equalizer needs the computation of only mean and variance that requires only $\mathcal{O}(Kn_t)$ per-symbol complexity. BCJR decoding was employed to decode the outer convolutional code. Simulation results demonstrated good coded BER performance for this turbo equalization scheme, which makes it attractive for severely delay spread MIMO-ISI channels like ultrawideband channels and underwater acoustic channels.

References

[1] D. Cassioli, M. Z. Win, and A. F. Molisch, "The ultra-wide bandwidth indoor channel: From statistical model to simulations," *IEEE Jl. Sel. Topics in Commun.* vol. 20, no. 6, pp. 1247-1257, August 2002.

[2] A. F. Molisch, J. R. Foerster, M. Pendergrass, "Channel models for ultrawideband personal area networks," *IEEE Wireless Commun.*, vol. 10, no. 6, pp. 14-21, December 2003.

[3] R. Saadane and A. M. Hayar, "DRB1.3 third report on UWB channel models," http://www.eurecom.fr/util/publidownload.fr.htm?id=2112, Newcom, November 2006.

[4] X. Geng and A. Zeilinksi, "An eigenpath underwater acoustic communication channel model," *Proc. MTS/IEEE OCEANS'95*, pp. 1189-1196, October 1995.

[5] H. Sari, G. Karam, and I. Jeanclaude, "Transmission techniques for digital terrestrial TV broadcasting," *IEEE Commun. Mag.,* vol. 33, no. 2, pp. 100-109, February 1995.

[6] D. Falconer, S. L. Ariyavisitakul, A. Benyamin-Seeyar, and B. Eidson, "Frequency domain equalization for single-carrier broadband wireless systems," *IEEE Commun. Mag.,* pp. 58-66, April 2002.

[7] Z. Wang, X. Ma, and G. B. Giannakis, "OFDM or single-carrier zero-padded block transmissions", *IEEE Trans. Commun.*, vol. 52, no. 3, pp. 380-394, March 2004.

[8] S. Ohno, "Performance of single-carrier block transmissions over multipath fading channels with linear equalization," *IEEE Trans. Signal Process.,* vol. 54, no. 10, pp. 3678-3687, October 2006.

[9] B. Devillers, J. Louveaux, and L. Vandendorpe, "About the diversity in cyclic prefixed single-carrier systems," *Physical Communications*, vol. 1, no. 4, pp. 266-276, December 2008.

[10] R. Dinis, R. Kalbasi, D. Falconer and A. Banihashemi, "Iterative layered space-time receivers for single-carrier transmission over severe time-dispersive channels," *IEEE Commun. Letters*, vol. 8, no. 9, pp. 579-581, September 2004.

[11] Y. Zhu and K. B. Letaief, "Single-carrier frequency-domain equalization with noise prediction for MIMO systems," *IEEE Trans. Commun.*, vol. 55, no. 5, pp. 1063-1076, May 2007.

[12] F. Pancaldi and G. M. Vitetta, "Frequency-domain equalization for space-time block-coded systems," *IEEE Trans. Wireless Commun.*, vol. 4, no. 6, pp. 2907-2916, November 2005.

[13] B. Ng, C. Lam, and D. Falconer, "Turbo frequency domain equalizer for single-carrier broadband wireless systems," *IEEE Trans. Wireless Commun.*, vol. 6, no. 2, pp. 759-767, February 2007.

[14] J. Luo, K. Pattipati, P. Willett, and F. Hasegawa, "Near-optimal multiuser detection in synchronous CDMA using probabilistic data association," *IEEE Commun. Letters*, vol. 5, no. 9, pp. 361-363, 2001.

[15] T. Wo and P. A. Hoeher, "Low-complexity Gaussian detection for MIMO systems," *Jl. of Electrical and Computer Engineering*, vol. 2010, article ID 609509, 12 pages. doi: 10.1155/2010/609509.

[16] R. Koetter, A. C. Singer, and M. Tuchler, "Turbo equalization," *IEEE Signal Proc. Mag.,* pp. 67-80, January 2004.